Efficient velocity model evaluation with multiple shots

Adam Halpert

ABSTRACT

An efficient method for quickly testing velocity models can be useful in the model-building workflow, especially if several discrete models are under consideration. Previous demonstrations of a scheme using Born-modeled wavefields have been limited by the requirement to image only sparsely-sampled locations in order to avoid crosstalk artifacts. Alternatively, performing multiple experiments in order to "fill in" a larger proportion of the image can overcome this limitation, at the expense of computational complexity. Tests on both synthetic and field data indicate that this may be a worthwhile tradeoff, especially since even a multi-shot approach is still much less expensive than a standard migration of the full dataset.

INTRODUCTION

Building an accurate seismic velocity model is essential for obtaining an acceptable image of the subsurface. When the subsurface is especially complex, for example in geological settings dominated by irregularly-shaped salt bodies, this task becomes particularly challenging. The large contrast between salt and sediment velocities magnifies the effects of inaccurate salt interpretation, resulting in a poor image. Unfortunately, velocity model-building is a time-consuming process that often requires several iterations. In situations where the top or (especially) base salt interpretation is uncertain or ambiguous, several different salt scenarios may be geologically feasible. Therefore, a means of quickly testing the effects of several different possible velocity models would be extremely useful for judging and refining salt interpretations. Various approaches to this problem have been proposed, many of which (e.g., Wang et al. (2008)) rely on fast migrations based on Gaussian beam imaging (Hill, 1990). Previously, I introduced a Born modeling and migration scheme that allows for fast remigrations of data synthesized from an initial image, while incorporating prestack velocity information from the initial image's subsurface offset gathers (Halpert and Tang, 2011; Halpert, 2012). Unfortunately, when using a single areal shot to image the synthesized data, crosstalk issues can arise unless only sparsely spaced image locations are used. While such an approach can still yield quantifiably useful information, a more complete image would provide additional information, and make it easier to form more qualitative judgments of image quality. Here, I explore methods for incorporating multiple areal shots into the imaging process.

In the following sections, I will review the Born modeling methodology and outline the procedure for obtaining the synthesized source and receiver wavefields mentioned above. I will then discuss strategies for incorporating data from multiple shots into the result, while avoiding crosstalk contamination. Using simple 2D synthetic models, I will show that the optimal strategy is to perform independent experiments using appropriately-spaced image locations, and then to combine the final images. Finally, I will demonstrate this method on a 3D field seismic dataset from the Gulf of Mexico. While the strategy I present here is less computationally efficient than using only a single shot to image the synthesized data, the improvement in the results image quality suggests it is a viable option to test velocity models in a way that remains much faster than performing full migrations.

SYNTHESIZED WAVEFIELDS

The goal of the model evaluation procedure is to use Born modeling (Stolt and Benson, 1986) to synthesize a new dataset that is much smaller than the original dataset used to generate an initial migrated image. Since the synthesized data can be "recorded" at any location in x, y, and even z, this procedure is effectively target-oriented. There are three basic steps needed to reach our goal of efficient velocity model evaluation:

1. Generate an areal source function using one or more subsurface offset gathers from the initial prestack image. Mathematically, this areal source is described as
$$S(\mathbf{x}_s, \omega) = \sum_{\mathbf{x}'} \sum_{\mathbf{h}} G^*_{v_0}(\mathbf{x}' - \mathbf{h}, \mathbf{x}_s, \omega) m(\mathbf{x}', \mathbf{h}), \tag{1}$$
where $\mathbf{x}_s = (x_s, y_s, z_s)$ are the arbitrarily defined locations where the wavefield will be recorded; $\mathbf{h}$ is the vector of subsurface half-offsets; ω is angular frequency; $\mathbf{x}'$ is the location of the exploding image point in the subsurface; and G_{v_0} is the Green's function connecting the source to the image point (here, * denotes the adjoint). The Green's function is computed using the same velocity model (v_0) that was used to image the originally-recorded data, meaning that the recorded wavefield should be independent of the original velocity model choice. However, since this velocity model is unlikely to be correct, the initial image should contain valuable information about the accuracy of this model in the form of subsurface offset gathers. Subsurface offset gathers from true-velocity images will have all energy focused at zero subsurface offset, while an incorrect velocity model will result in a "smearing" of energy to nonzero offsets (Biondi, 2005). Thus, the inclusion of the subsurface offset term $\mathbf{h}$ in equation 1 is designed to incorporate this information into the modeling.

2. Using the new source function and a reflectivity model based on the initial image, employ Born modeling to generate a new dataset with acquisition geometry best suited to image the target area. To do this, I define the simulated dataset

d' recorded at arbitrary receiver locations $\mathbf{x}'_r$:

$$d'(\mathbf{x}_r, \omega) = \sum_{\mathbf{x}'} \sum_{\mathbf{h}} \Gamma(\mathbf{x}_s, \mathbf{h}, \omega) G_{v_0}(\mathbf{x}' + \mathbf{h}, \mathbf{x}'_r, \omega) m(\mathbf{x}', \mathbf{h}). \tag{2}$$

Here, m is the reflectivity model (in our case, the initial image), and the Γ term is defined as

$$\Gamma(\mathbf{x}_s, \mathbf{h}, \omega) = \sum_{\mathbf{x}_s} S(\mathbf{x}_s, \omega) G_{v_0}(\mathbf{x}_s, \mathbf{x}' - \mathbf{h}, \omega), \tag{3}$$

where S is as defined in equation 1. Crucially, the Green's functions in equations 1 and 2 are computed using the same velocity model - the one used to generate the initial image. As proven in Tang (2011), this means that the "data" synthesized using equation 2 will be kinematically invariant of this initial velocity model. Even though this model is likely to be wrong, we can still confidently make use of the data synthesized from it.

3. Migrate the simulated data obtained in Step 2, using the source function from Step 1. We can produce an image using standard wave-equation migration techniques:

$$m'(\mathbf{x}', \mathbf{h}) = \sum_{\omega} G^*_{v_1}(\mathbf{x}' - \mathbf{h}, \omega) \sum_{\mathbf{x}_r} G{v_1}^*(\mathbf{x}' + \mathbf{h}, \mathbf{x}'_r, \omega) d'(\mathbf{x}_r, \omega). \tag{4}$$

This step is extremely computationally efficient compared to a full migration of the original data, allowing for testing of several possible velocity models in a fraction of the time it would take to evaluate them using standard migration techniques. It is important to note that the Green's functions in equation 4 can be computed using any velocity model (v_1), and not necessarily the same one used to generate the source and receiver wavefields in previous steps. This can allow for testing of multiple possible velocity models.

Unfortunately, performing the above steps in a single iteration (i.e., using a single areal shot to migrate the synthesized dataset) can allow crosstalk artifacts to contaminate the final image. For example, these artifacts can arise when the data used to generate the synthesized wavefields overlap in the subsurface offset domain. The artifacts can be avoided as long as only appropriately spaced image locations are used to generate the wavefields. In Figure 2, image locations along the flat reflector seen in Figure 1 are spaced at an increment of twice the maximum subsurface offset used to synthesized the new wavefields. The result clearly shows the the velocity model used to image the wavefields in panel a (which in this example was the same used to create the initial image) is too slow compared to the true velocity used in panel b. However, if the image locations are spaced too close together, crosstalk artifacts lead to severe degradation of the image (Figure 3). Even though the slower velocity model is used in this example, the artifacts make it impossible to judge the accuracy of the model.

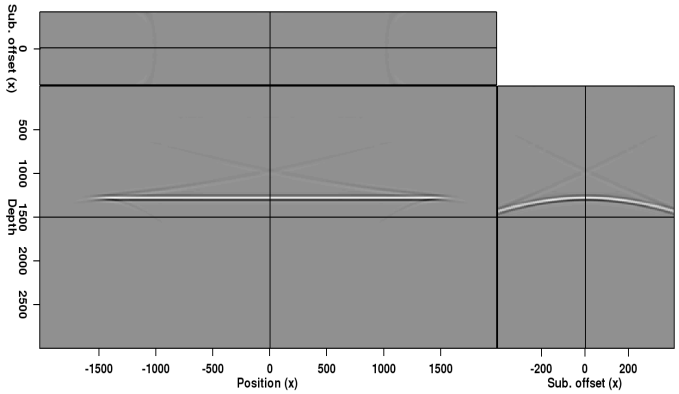

Figure 1: Initial image of a flat reflector used to demonstrate the model evaluation procedure. Note that this image was migrated using an incorrect (slow) velocity model. [**CR**]

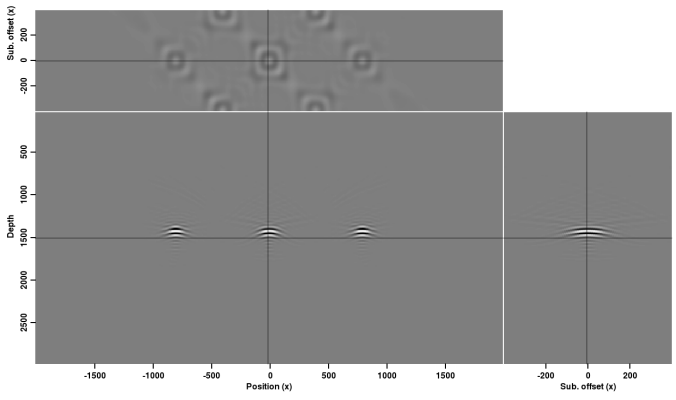

(a)

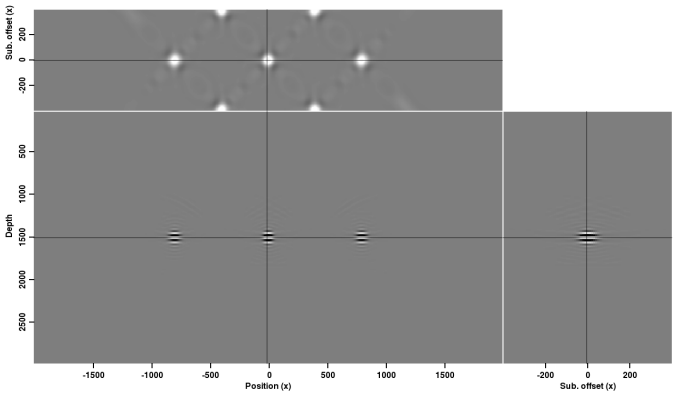

(b)

Figure 2: Result of imaging the Born-modeled dataset derived from widely-spaced locations along the reflector in Figure 1, using (a) a velocity model that is too slow, and (b) the true velocity model. Even though the initial image was also migrated using the slow velocity, these results clearly identify the correct model. [**CR**]

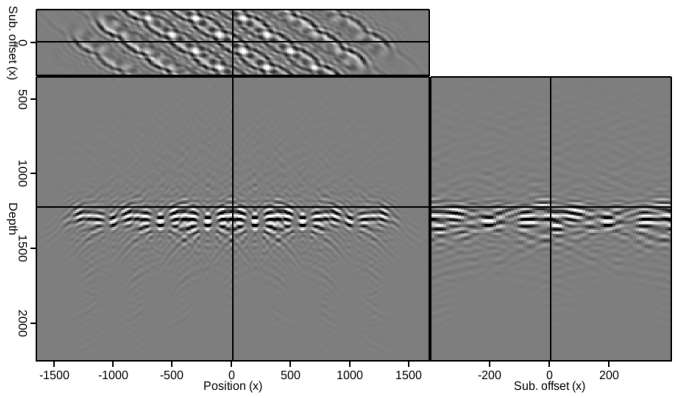

Figure 3: Result analagous to Figure 2(a), but if image locations are spaced too close together. Crosstalk artifacts from overlapping data in the subsurface offset domain severely contaminate the image, making any judgments about the accuracy of the velocity model used to generate the image nearly impossible. [**CR**]

USING MULTIPLE SHOTS

One way to mitigate the crosstalk artifacts seen in Figure 3 is to synthesize multiple source and/or receiver wavefields, which illuminate different locations along the reflector. For example, in Figure 4(a), the isolated locations from the initial image are too close together, resulting in the crosstalk-contaminated result in Figure 3. However, the same image locations may be represented as the union of the locations in Figures 4(b) and 4(c), both of which feature spacings sufficient to avoid crosstalk artifacts. This is demonstrated in Figure 5, in which the datasets synthesized from the corresponding images in Figures 4(b) and 4(c) have clearly been imaged with the slower velocity. The goal of using multiple shots is to achieve a more informative result than those from the two sub-images in Figure 5, while mitigating the crosstalk artifacts that would arise if this were attempted with a single shot.

The equations in the previous section suggest that there are three possible opportunities to combine information from multiple experiments into a single result. The first option is to create a source wavefield for each set of locations being imaged, and then summing them before modeling the receiver wavefield. This would change the expression for the source wavefield to

$$S(\mathbf{x}_s,\omega) = \sum_I \sum_{\mathbf{x}'} \sum_{\mathbf{h}} G^*_{v_0}(\mathbf{x}'-\mathbf{h},\mathbf{x}_s,\omega,I) m(\mathbf{x}',\mathbf{h},I), \tag{5}$$

where I is now a single experiment using sufficiently-spaced image locations.

The second option for utilizing multiple experiments is to synthesize separate receiver wavefields corresponding to each source wavefield, and then combining the receiver wavefields prior to imaging. This would alter the expression for the Born-

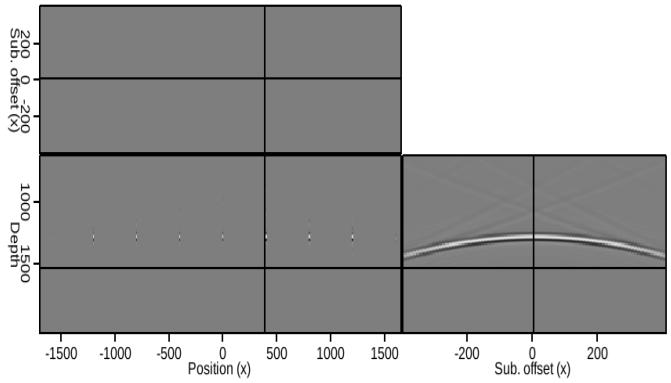

(a)

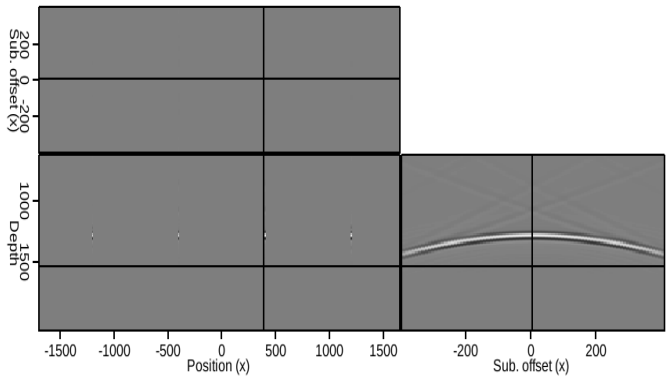

(b)

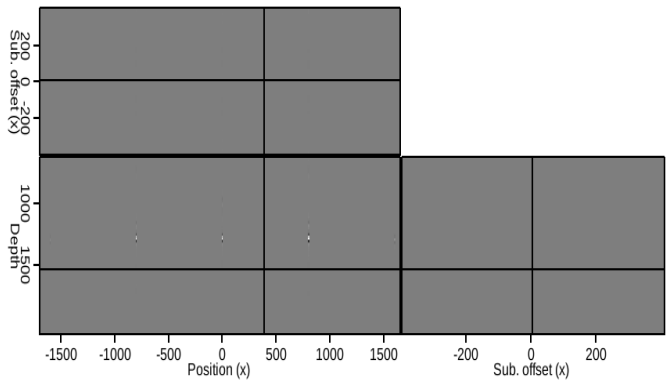

(c)

Figure 4: Isolated locations from the reflector imaged in Figure 1. When used to synthesize the Born-modeled dataset, the points in panel (a) are too densely sampled to avoid crosstalk contamination, while those in (b) and (c) are sufficiently sparse. [**CR**]

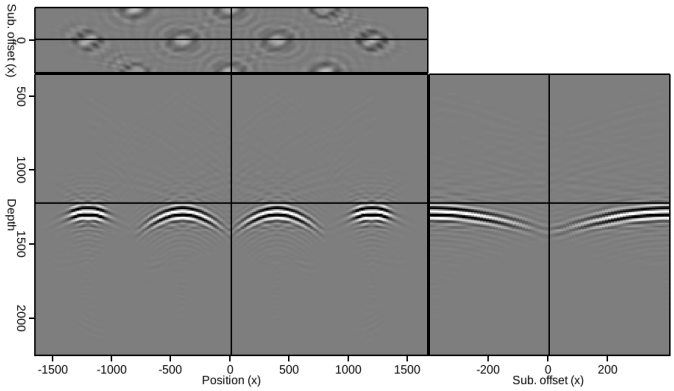

(a)

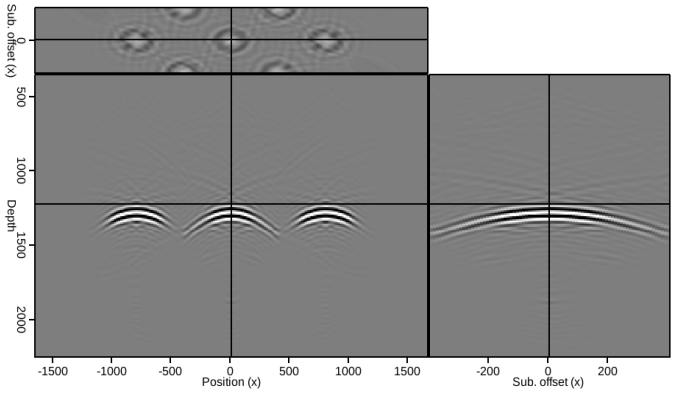

(b)

Figure 5: Results of imaging the datasets derived from the images in Figure 4(b) (panel a) and Figure 4(c) (panel b). It is clear that the slower velocity model was used. [**CR**]

modeled wavefield to

$$d'(\mathbf{x}_r, \omega) = \sum_I \sum_{\mathbf{x}'} \sum_{\mathbf{h}} \Gamma(\mathbf{x}_s, \mathbf{h}, \omega, I) G_{v_0}(\mathbf{x}' + \mathbf{h}, \mathbf{x}'_r, \omega, I) m(\mathbf{x}', \mathbf{h}, I), \tag{6}$$

where I is again an individual set of image locations and the Γ term is defined as

$$\Gamma(\mathbf{x}_s, \mathbf{h}, \omega, I) = \sum_{\mathbf{x}_s} S(\mathbf{x}_s, \omega) G_{v_0}(\mathbf{x}_s, \mathbf{x}' - \mathbf{h}, \omega, I). \tag{7}$$

Unfortunately, Figure 6 demonstrates that neither of these approaches will mitigate the crosstalk artifacts. In fact, the images are nearly indistinguishable from each other or from the single-experiment result in Figure 3. The presence of overlapping data from the subsurface offset domain leads to crosstalk issues in the imaging step, no matter at what point that overlapping data is introduced to the process.

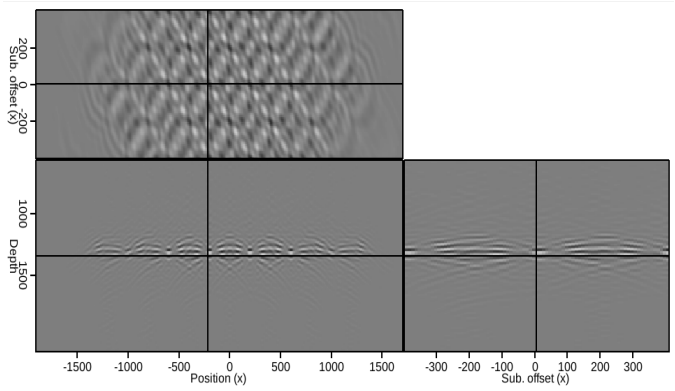

(a)

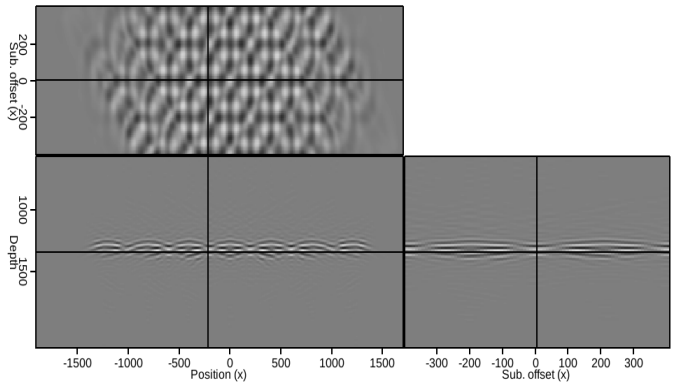

(b)

Figure 6: Result of imaging wavefields generated using (a) multiple source wavefields summed into a single wavefield, and (b) multiple source and receiver wavefields which are summed before imaging. Neither approach mitigates the extrememly prevalant crosstalk artifacts. [**CR**]

Finally, the third option is also the simplest: image the source and receiver wavefields separately for each set of image locations, and sum the resulting images into

a single result. While this approach is less computationally efficient than the first two, it is still far less expensive than performing full migrations, especially for 3D datasets. Figure 7(a) shows that this approach does indeed eliminate the crosstalk artifacts, and provides meaningful information about the (slow) velocity model used. Furthermore, using the true velocity model to image the synthesized datasets (Figure 7(b)) illustrates the effectiveness of this method for identifying more accurate velocity models.

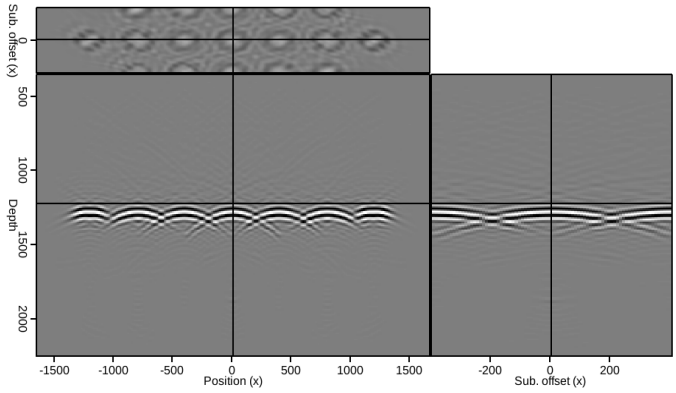

(a)

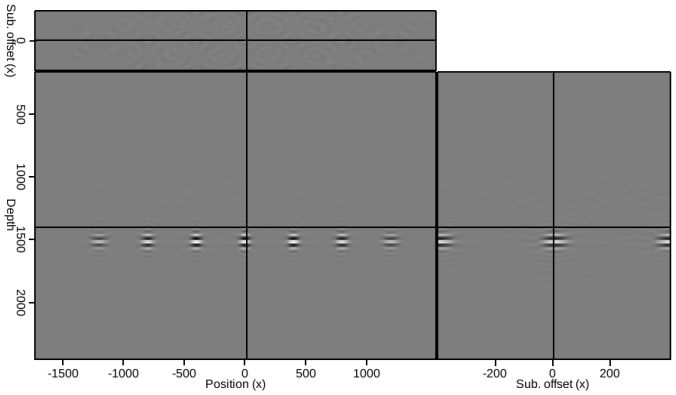

(b)

Figure 7: Results of summing individual images corresponding to datasets created using the images in Figures 4(b) and 4(c) with (a) slow velocity, and (b) true velocity. Now, the accuracy of the velocity model can be judged without interfering crosstalk artifacts. [**CR**]

Dipping reflector

The advantages of this method can be seen even more clearly in the case of a dipping reflector, such as the 40° one imaged with a too-slow velocity in Figure 8. If the locations used to generate the source and receiver wavefields in a single experiment are too densely sampled, the resulting image (Figure 9) is severely contaminated by crosstalk artifacts. However, creating appropriately-sampled images separately, and

then summing them, provides a much clearer and more interpretable result (Figure 10(a)). Now, it is apparent that a slow migration velocity has been used. When the true velocity is used to image the wavefields (Figure 10(b)), the summed image noticeably improves. Further improvement can be realized if the entire reflector is utilized in various experiments, which are then summed to give a final image (Figure 11). Although other imaging artifacts are somewhat obscuring the reflector, it is still clearly visible. Results such as this one may be obtained at a fraction of the cost of a full migration.

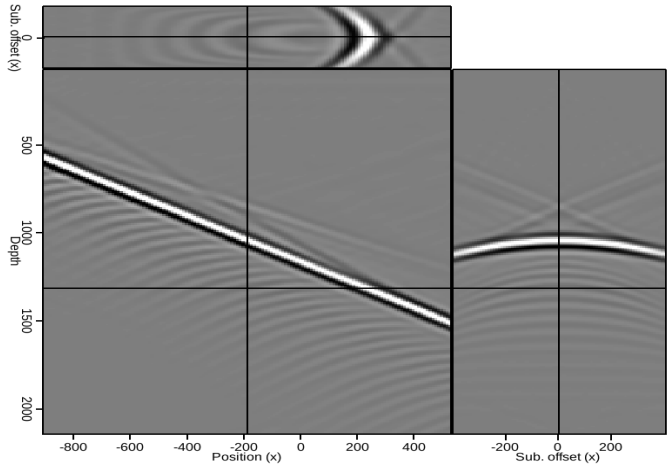

Figure 8: A 40° dipping reflector that has been imaged with a too-slow velocity model. [**CR**]

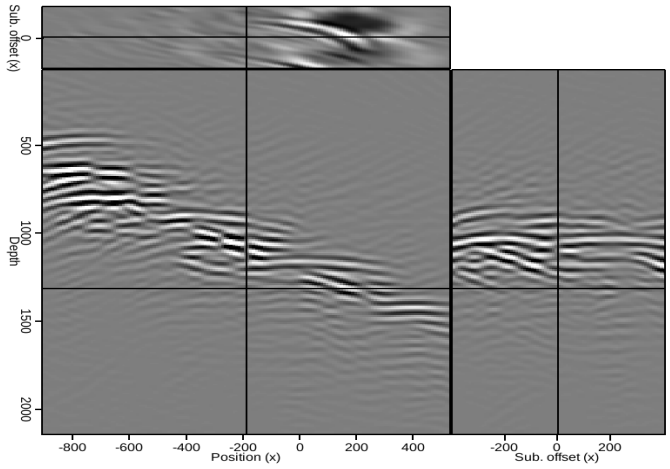

Figure 9: When image locations used to synthesize new source and receiver wavefields are too densely sampled, severe crosstalk artifacts degrade the image. [**CR**]

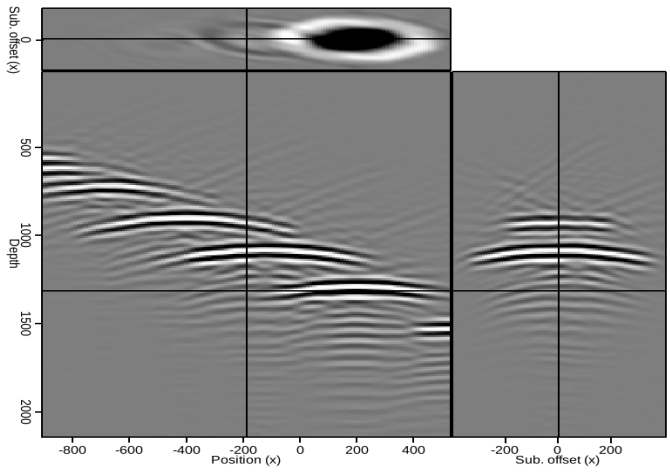

(a)

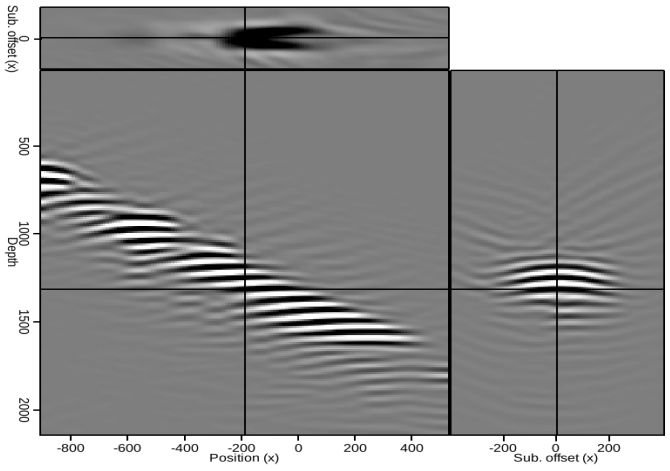

(b)

Figure 10: Result of summing several images derived from sparsely-sampled locations along the dipping reflector using the (a) slow and (b) true migration velocity for the final imaging step. [**CR**]

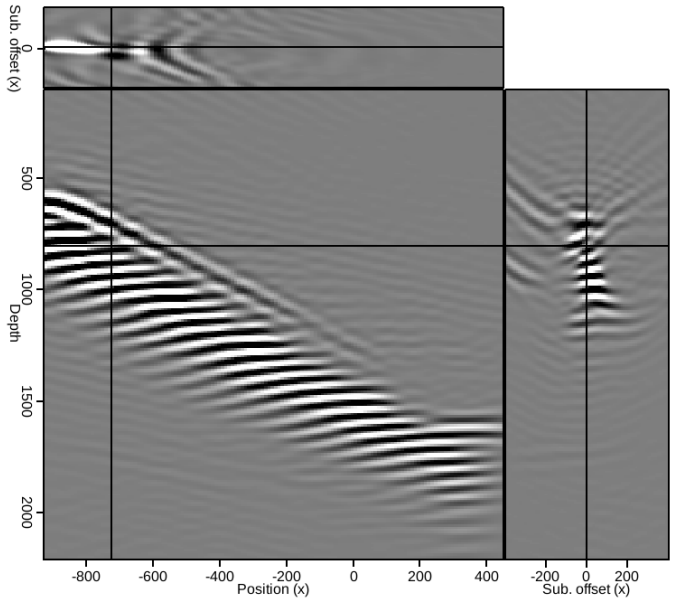

Figure 11: Image obtained using locations along the entire dipping reflector. While imaging artifacts somewhat obscure the reflector in the final image, the image still provides interpretable information at a fraction of the cost of a full migration. [**CR**]

FIELD DATA TEST

Now, the multi-shot procedure outlined above will be tested on a 3D, wide-azimuth dataset from the Gulf of Mexico, provided by Schlumberger Multiclient. For field data, an interpreter chooses a reflector of interest to use for the model evaluation procedure; in Figure 12, the base salt reflector has been chosen because it should be highly susceptible to changes in salt geometry. Those changes may be seen by comparing the velocity models in Figure 13. Panel a is the velocity model provided with the data, and panel b was modified via 3D interpreter-guided image segmentation (Halpert et al., 2014). The most noticeable differences are the isolation of an inclusion near the top of the salt body, and a re-interpretation of the base salt to make it shallower.

Results from performing 15 separate experiments, and summing the images together, are seen in Figure 14. By using multiple experiments to form the image, we gain a far greater degree of detail into the reflector's behavior than if just one or two image locations had been used. It is important to note that, even though many experiments were performed to obtain these images, the total computational expense was still far less (and required a less powerful computer) than generating a full image such as the one in Figure 12. While it is difficult to form a qualitative judgment about which model is more accurate simply from these images, more quantitative methods such as the focusing measure discussed in Halpert (2012) can allow interpreters greater insight into five-dimensional volumes such as these.

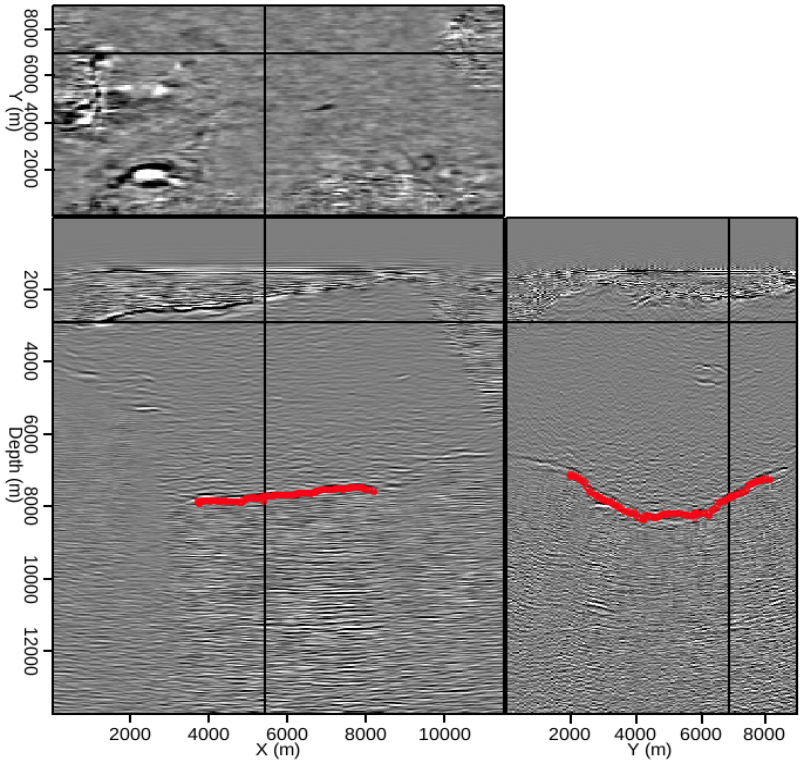

Figure 12: Portion of an image from a 3D Gulf of Mexico dataset. The indicated base salt reflector will be used for the efficient velocity model testing procedure. [**CR**]

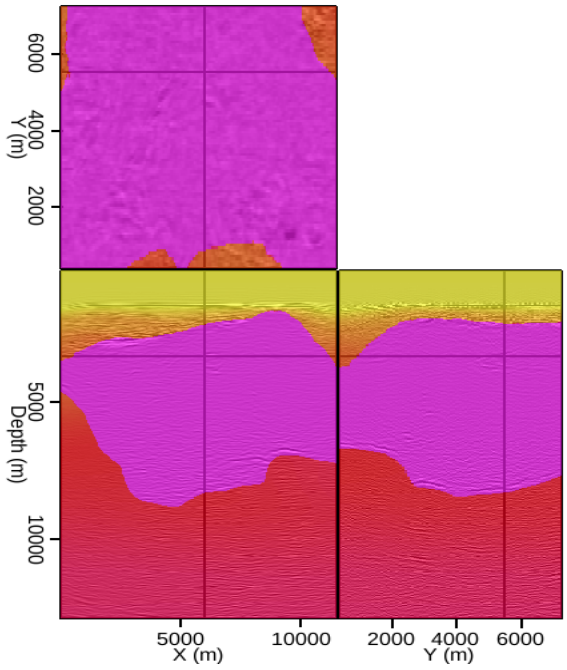

(a)

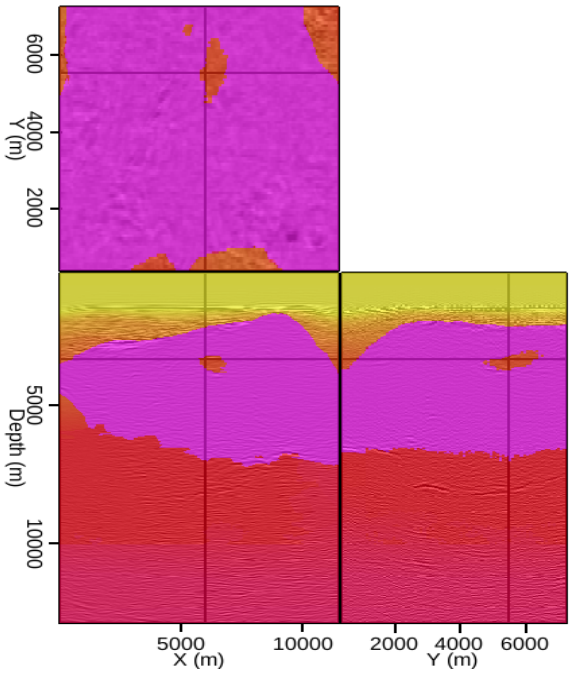

(b)

Figure 13: (a) Original and (b) updated velocity models to be tested. The model in (b) isolates a salt inclusion and a re-interpreted base salt, and was obtained via interpreter-guided image segmentation. [**CR**]

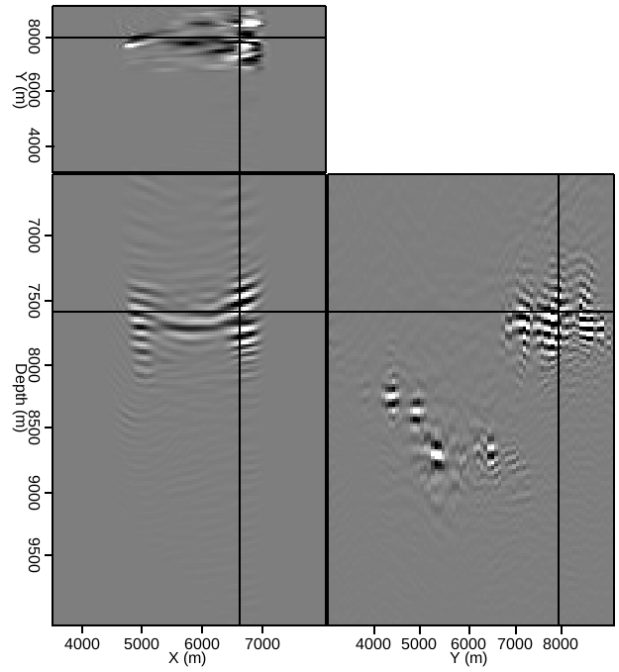

(a)

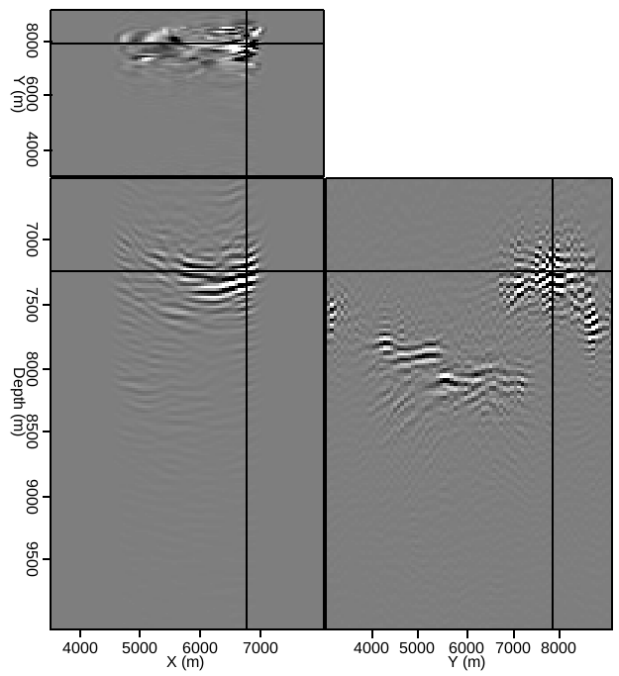

(b)

Figure 14: Results after summing images using 15 locations along the indicated reflector in Figure 12 for synthesizing wavefields. The image in (a) used the provided velocity model in Figure 13(a), while the new model in Figure 13(b) was used for (b). [**CR**]

CONCLUSIONS

Using synthesized wavefields derived from an initial model is an effecient way to quickly test velocity models, but a single experiment is limited to sparsely sampled locations along a reflector to avoid contamination from crosstalk artifacts. Although there is a trade-off in computational expense, this limitation can be lifted by performing several imaging experiments, and summing the resulting images. This allows for a more complete picture of the reflector to emerge, providing a more interpretable result. This approach can also allow for a full reconstruction of the reflector if the full extent of the initial image is used to synthesize wavefields; however, this is unlikely to be necessary for an acceptable result.

ACKNOWLEDGMENTS

I am grateful to Schlumberger Multiclient for providing the field dataset used here, and to Yaxun Tang for his invaluable assistance with building the Born modeling/imaging framework.

REFERENCES

Biondi, B., 2005, 3D seismic imaging: Stanford University.

Halpert, A., 2012, Fast velocity model evaluation with synthesized wavefields: SEP-Report, **147**, 39–48.

Halpert, A., R. Clapp, and B. Biondi, 2014, Salt delineation via 3D interpreter-guided seismic image segmentation: Interpretation, **2**, T79–T88.

Halpert, A. and Y. Tang, 2011, Velocity model evaluation through Born modeling and migration: a feasibility study: SEP-Report, **145**, 15–26.

Hill, N. R., 1990, Gaussian beam migration: Geophysics, **55**, 1416–1428.

Stolt, R. H. and A. Benson, 1986, Seismic migration: Theory and practice: Geophysical Press.

Tang, Y., 2011, Imaging and velocity analysis by target-oriented wavefield inversion: PhD thesis, Stanford University.

Wang, B., J. Ji, C. Mason, S. Gajawada, and Y. Kim, 2008, Beam-based interactive imaging for salt interpretation and salt model building: SEG Technical Program Expanded Abstracts, **27**, 3073–3077.